Proceedings of the ASME 2019 38th International Conference on Ocean, Offshore and Arctic Engineering
OMAE2019
June 9-14, 2019, Glasgow, Scotland, UK

OMAE2019-95474

COMPONENT-BASED MODELING AND SIMULATION OF NONLINEAR DRILL-STRING DYNAMICS

Njål Tengesdal*
Dept. of Mech. and Ind. Eng.
NTNU Norwegian U. of Sci. and Tech.
NO-7491 Trondheim
Norway
Email: njaal.tengesdal@ntnu.no

Christian Holden
Dept. of Mech. and Ind. Eng.
NTNU Norwegian U. of Sci. and Tech.
NO-7491 Trondheim
Norway
Email: christian.holden@ntnu.no

Eilif Pedersen
Dept. of Marine Tech.
NTNU Norwegian U. of Sci. and Tech.
NO-7491 Trondheim
Norway
Email: eilif.pedersen@ntnu.no

ABSTRACT

In this paper, we present a dynamic model for a generic drill-string. The model is developed with the intention for component-based simulation with coupling to external subsystems. The performance of the drill-string is vital in terms of efficient wellbore excavation for increased hydrocarbon extraction. Drill-string vibrations limit the performance of rotary drilling; the phenomenon is well-known and still a subject of interest in academia and in industry. In this work, we have developed a nonlinear flexible drill-string model based on Lagrangian dynamics, to simulate the performance during vibrations. The model incorporates dynamics governed by lateral bending, longitudinal motion and torsional deformation. The elastic property of the string is modeled with mode shape functions representing the elastic deformation, with a finite set of modal coordinates. By developing a bond graph model from the equations of motion, we can ensure correct causality of the model towards interacting subsystems. The model is analyzed through extensive simulations in case studies, comparing the qualitative behavior of the model with state-of-the art models. The flexible drill-string model presented in this paper will aid in developing simulation case studies and parameter identification for offshore drilling operations.

Keywords: Offshore drilling, Drill-string dynamics, Nonlinear vibrations, Lagrangian dynamics, Bond graphs

*Address all correspondence to this author.

INTRODUCTION

The drill-string is a vital component of a drilling rig multi-domain system, and crucial in establishing the wellbore for hydrocarbon extraction. A drill-string consists of individual pipes joined together by tool joints, stabilizers to center the pipe in the wellbore, measurement-while-drilling (MWD) tools, and sensor wiring. This structure can be several kilometers long. A generic model of the drill-string assembly is seen in Fig. 1.

The string is suspended in the derrick to the top drive, moving upwards when tripping out of hole, and downwards during drilling and run-in of new pipe stands. The lower section of the string, consisting of drill collars and the bit, is commonly referred to as the bottom hole assembly (BHA). The drill collar section is a set of heavier pipes to produce enough weight on bit (WOB) when drilling and intervals of stabilizers keeping the string centred in the borehole. The torque on the bit is a consequence of the applied torque at the top, WOB, and the torque from the formation being excavated due to cuttings (cuttings from the rock smashed by the bit due to rotation) and the friction from the rock it self [1].

The drill-string classifies as a flexible slender object [2]. In general, large vibrations are a problem, and in terms of drilling there exist three distinct vibration modes:

a. Torsional vibrations, occurring along the string or at the bit where the torque in the drill-string must overcome the static torque from the formation to break free. This result in periodic oscillatory behavior referred to as ”stick-slip” [3, 4].

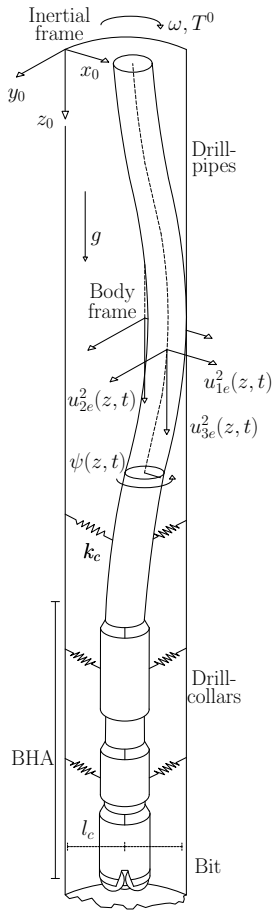

FIGURE 1. A DRILL-STRING ASSEMBLY WITH NOTATIONS.

b. Axial, compression, or longitudinal vibrations, also referred to as "bit-bounce". This occurs when the bit periodically comes loose from the formation [5].
c. Lateral vibrations, also called whirling motion. Along the length of the string the whirling motion tends to cause an uneven pattern in the well trajectory, and can potentially result in formation fracture in the wellbore [5].

For the drill-string, vibrations can result in extensive wear or failure of the bit and other components in the assembly [5]. The vibration modes have been subject to extensive research for both understanding and mitigation through new control strategies.

Modeling and simulation of drill-string dynamics is a large research field, and subsequently a large number of models for analyzing vibrations exist. An important contribution in the research field of drill-string vibrations is the work of Kyllingstad and Halsey [3]. The research in [3] concerns the string torsional vibrations induced by stick-slip. The vibrations are modeled as a transmission line reflecting the torsional waves created by the stick-slip friction.

Commonly found in control applications are low-order ordinary differential equation (ODE) models, confined to vertical well applications. In [6] a lumped model approach is used, representing each string section as a mass-spring-damper object, for both axial and torsional modes. The focus in [6] is analysis of the effect of a down-hole bit-rock interaction model. These models are suitable of real-time applications, but are confined to uncoupled vibrations.

Christoforou and Yigit [7] have developed a coupled second order model with axial, torsional, and lateral dependency with the objective of mitigation of vibrations. The model is developed under the assumption of one-mode approximation, and the dependency for the coupled vibrations is created by the bit-rock friction model. A first-mode approximation is made, discretizing the assembly as two mass points. The coupling arises from bore-hole wall and bit-rock interaction.

Tucker and Wang [4] model the drill-string dynamics as an elastic rod with Cosserat theory. This method implies sectioning the rod into finite elements with unit vectors, each representing bending or twist, shear stress, and axial motion along the rod length. The model then consists of a set of nonlinear partial differential equations (PDE).

Jansen [5] analytically derived model equations for the vibrations listed above for sections of the drill-string (collar etc.) and also uses a finite element model (FEM) as foundation for analyzing the vibration stages of a drill-string. Jansen also presented a computer simulation program for a nonlinear drill-string model. A FEM is favorable in terms of close-to-real results in applications but often requires large computational power and significant analysis time [8].

Bakhtiari-Nejad and Hosseinzadeh [9] modeled the string dynamics by solving the PDE for axial and torsional motion. This is further lumped by using a Ritz-series expansion with assumed modes to represent the vibrations. The string interacts with the bit-rock model from [10].

Hovda [11] presents an axial model of a drill-string assembly with a finite number of discrete mass-spring-damper elements. Unlike the above-mentioned work, this model incorporates the skin-friction arising from the mud-flow in the annulus of the well. This is included to account for surge and swab effects arising from the vessel heave motion. The work presents a semi-analytical approach, being favorable in terms of real-time applications and model calibration towards field data.

Ritto et al. [2] presents a nonlinear model of a drill-string assembly, including a stochastic model for the bit-rock interaction. This approach is shown to account for uncertainties in the bit-rock model, which in general is hard to predict with deterministic models. A similar stochastic approach is applied to model lateral vibrations in [8].

In the view of component-based modeling, the framework of bond graph (BG) modeling plays a significant role. The structure creates a unified approach for multi-domain systems, and

allows for graphical modeling. An overview of this tool is found in [12]. In Pedersen and Polic [13] a bond graph model framework for rotordynamic applications is developed. The resemblance between this and the current work is evident and as such the current model development is a formal extension to this bond graph model framework.

In terms of bond graph applications for drill-string modeling, Sarker et. al. [14] presents a lumped-section model for axial and torsional motion. The bond graph model is comprised of element sections represented by rigid bodies, and the elasticity is modeled by coupled torsional, axial and bending springs between each body. The model is used to analyze drill-string behavior in horizontal wells, and predicts the whirl phenomena close to the BHA together with the coupling effect for axial and torsional motion trough the bit-rock model.

In this paper, we derive a distributed-parameter model in terms of the floating frame of reference formulation, taking advantage of mode shape functions to describe the elastic deformation. The modeling framework is useful for establishing a component-based model of a generic drill-string, undergoing deformation. The mode shape functions are derived by solving the eigenvalue problem for a fixed-free Euler Bernoulli beam, longitudinal bar and a shaft. We investigate the effect of including torsional deformation and the effect of nonlinear coupling between the elastic and rigid motion through simulation case studies. To the best of the authors' knowledge, using the floating reference frame formulation for describing the coupling between lateral and torsional deformation and structuring this in a component-based model for a drill-string, has not been previously presented.

MODELING

We assume that no rotation of the drive machinery occurs due to the fixation to the dolly guides. The dolly guides are the vertical rails which the top drive is fixed to in the derrick tower. Furthermore, we assume a vertical well profile and that the assembly consists of drill-pipes.

A general drill-string assembly being subject to lateral motion is illustrated Fig. 1. With Fig. 1 as a starting point, we consider an inertial frame located in space, a body frame attached to a pipe disc element, and a deformed configuration in frame $\{x,y,z\}_2$. These frames are denoted $\{x,y,z\}_0$, $\{x,y,z\}_1$, and $\{x,y,z\}_2$, respectively. The frame and vector definitions are shown in Fig. 2. We assume that the elastic, deformed element is skewed in the horizontal plane, with no rotation around the x and y axes. This assumption simplifies the analysis, since both pitch and roll (inclination and azimuth) of the element is neglected. This is reasonable in the current case, considering a vertical well.

This formulation is known as the floating reference frame formulation [15]. This gives two sets of coordinates, one describing the rigid body motion, along with the coordinates describing the elastic deformation. Additionally, we investigate the effect of

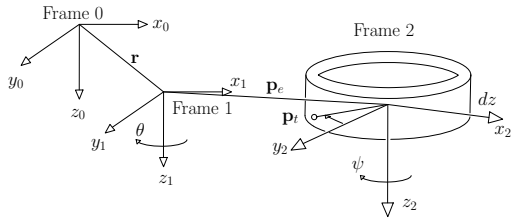

FIGURE 2. FRAME DEFINITIONS.

coupling the lateral deformation to twisting of the pipe due to torsion.

We start by defining the position of the pipe segment in space and the transformations occurring in the system, to finally derive the velocity of a point on the pipe element, subjected to elastic deformation. The position of body frame $\{1\}$ relative to inertial frame $\{0\}$ is given by $\mathbf{r} = [x,y,z]^\top$, where the bold notation is used for matrices and vectors. The rotation matrices from frame $\{0\}$ to $\{1\}$ and $\{1\}$ to $\{2\}$ are given as

$$\mathbf{R}_1^0(\theta(t)) = \begin{bmatrix} \mathrm{c}\theta & -\mathrm{s}\theta & 0 \\ \mathrm{s}\theta & \mathrm{c}\theta & 0 \\ 0 & 0 & 1 \end{bmatrix}, \ \mathbf{R}_2^1(\psi(z,t)) = \begin{bmatrix} \mathrm{c}\psi & -\mathrm{s}\psi & 0 \\ \mathrm{s}\psi & \mathrm{c}\psi & 0 \\ 0 & 0 & 1 \end{bmatrix} \quad (1)$$

where $\mathrm{c}\theta = \cos\theta$, $\mathrm{s}\theta = \sin\theta$, $\theta(t)$ is the rotation angle from $\{0\}$ to $\{1\}$ and $\psi(z,t)$ is the rotation angle from $\{1\}$ to $\{2\}$ about the z axis, given in terms of both space and time.

The position of an arbitrary twisted point $\mathbf{p}_t^0$ in frame $\{2\}$ expressed in $\{0\}$ is given by

$$\mathbf{p}_t^0 = \mathbf{r} + \mathbf{R}_1^0 \left(\mathbf{p}_e^1 + \mathbf{R}_2^1 \mathbf{p}_t^2 \right) \quad (2)$$

where $\mathbf{p}_e^1 = \left[u_{1e},\, u_{2e},\, u_{3e} \right]^\top$ is the position of the origin of frame $\{2\}$, $\mathbf{p}_t^2$ is the position of a point undergoing torsion, and subscripts e,t refers to elastic and torsion, respectively. The twisted pipe material point $\mathbf{p}_t^2$ has an additional angle $\psi(z,t)$ due to torsional deformation, being illustrated in the x, y plane in Fig. 3.

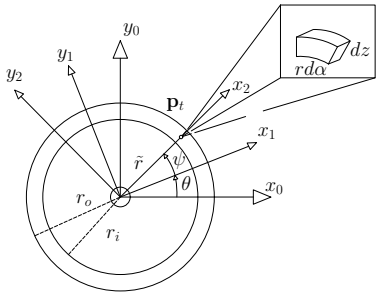

FIGURE 3. PLANE VIEW OF THE PIPE ELEMENT.

From Fig. 3, we can define the vector describing the twisted point $\mathbf{p}_t^2 = \left[\tilde{r},\, 0,\, 0\right]^\top$, where $\tilde{r}$ is the averaged radius of the pipe.

The time derivative of a material point on the pipe element is derived as

$$\dot{\mathbf{p}}_t^0 = \dot{\mathbf{r}} + \left(\mathbf{B}_\theta + \mathbf{S}_{\psi\theta}\right)\dot{\theta} + \mathbf{S}_\psi \frac{\partial \psi}{\partial t} + \mathbf{R}_1^0 \dot{\mathbf{p}}_e^1, \tag{3}$$

$$\text{where} \quad \mathbf{B}_\theta = \frac{\partial \mathbf{R}_1^0}{\partial \theta}\mathbf{p}_e^1,\ \mathbf{S}_\theta = \frac{\partial \mathbf{R}_1^0}{\partial \theta}\mathbf{R}_2^1\mathbf{p}_t^2,\ \mathbf{S}_\psi = \mathbf{R}_1^0 \frac{\partial \mathbf{R}_2^1}{\partial \psi}\mathbf{p}_t^2$$

and $\dot{\mathbf{p}}_t^2 = 0$ since $\tilde{r}$ is constant, and $\dot{\mathbf{R}} = \frac{\partial \mathbf{R}}{\partial \theta}\dot{\theta}$.

The flexibility of the pipe is represented by the elastic deformation $\mathbf{p}_e^1(z,t)$ and $\psi(z,t)$. These vectors can be described utilizing mode shape functions obtained from solving the eigenvalue problem of lateral bending by means of the Euler-Bernoulli beam model, longitudinal vibration of a bar and torsional vibration of a shaft. The mode shape functions are then defined by a set of fixed-free boundary conditions according to [16], where we obtain an infinite number of mode shapes in the x, y, z and ψ direction. The argument for using fixed-free boundaries are that the drill-string assembly is fixed in the top-drive.

Drill-strings are in general long, and therefore the mode shapes are normalized according to [13]. The mode shapes for lateral deformation grow without bounds when $z \to \infty$, due to the hyperbolic functions. We derive the mode shapes in terms of the normalized coordinate $s = z/L$ in nondimensional form. For the lateral bending modes, this yields

$$\begin{aligned} N_{n,x}(s) = N_{n,y}(s) &= \cos(\beta_n s) - \cosh(\beta_n s) \\ &-(\sin(\beta_n s) - \sinh(\beta_n s))\frac{\cos(\beta_n)+\cosh(\beta_n)}{\sin(\beta_n)+\sinh(\beta_n)} \end{aligned} \tag{4}$$

where n is the mode shape number and β is the root of the individual characteristic equation (see [16] for reference), determined out from the boundary conditions. The longitudal and torsional mode shape functions are given by

$$N_{n,z}(s) = \sin\left(\frac{(2n+1)\pi}{2}s\right),\ Y_{n,z}(s) = \sin\left(\frac{(2n+1)\pi}{2}s\right). \tag{5}$$

Furthermore, we evaluate the spatial variables $\mathbf{p}_e^1(z,t)$ and $\psi(z,t)$ by applying the Raleigh-Ritz approximations

$$u_{j,e}(z,t) \approx \sum_{k=1}^{n_j} N_{kj}(z) q_{kj}(t) \tag{6}$$

$$\psi(z,t) \approx \sum_{k=1}^{n_r} Y_k(z) q_k(t) \tag{7}$$

where the subscript r is for rotation, $j \in \{x, y, z\}$ and each spatial coordinate is a sum of n_j and n_r mode shapes multiplied with n_j and n_r generalized time-dependent coordinates. We rearrange (6) and (7) in vector form as

$$\mathbf{p}_e^1 = \begin{bmatrix} \mathbf{N}_x & \mathbf{0} & \mathbf{0} \\ \mathbf{0} & \mathbf{N}_y & \mathbf{0} \\ \mathbf{0} & \mathbf{0} & \mathbf{N}_z \end{bmatrix} \begin{bmatrix} \mathbf{q}_x \\ \mathbf{q}_y \\ \mathbf{q}_z \end{bmatrix} = \mathbf{N}\mathbf{q}_e,\ \psi(z,t) = \mathbf{Y}\mathbf{q}_\psi \tag{8}$$

where $\mathbf{N}_j$ are row vectors, $\mathbf{q}_j = \left[q_{1j},\, q_{2j},\, \ldots\, q_{n_j j}\right]^\top$, $\mathbf{q}_e = \left[\mathbf{q}_x^\top,\, \mathbf{q}_y^\top,\, \mathbf{q}_z^\top\right]^\top$ and $\mathbf{q}_\psi = \left[q_1,\, q_2,\, \ldots\, q_{n_r}\right]$ are column vectors with time dependent generalized coordinates, and the mode shape matrix $\mathbf{N}$ and vector $\mathbf{Y}$ are defined as

$$\mathbf{N} = \begin{bmatrix} N_{1x} & N_{2x} & \ldots & N_{n_1 x} & \mathbf{0} & \mathbf{0} \\ \mathbf{0} & N_{1y} & N_{2y} & \ldots & N_{n_2 y} & \mathbf{0} \\ \mathbf{0} & \mathbf{0} & N_{1z} & N_{2z} & \ldots & N_{n_3 z} \end{bmatrix}, \qquad \mathbf{Y} = \begin{bmatrix} Y_1 \\ Y_2 \\ \vdots \\ Y_{n_r} \end{bmatrix}^\top \tag{9}$$

where the total amount generalized coordinates for the mode shapes is then $n_{\text{modes}} = n_e + n_r$, where $n_e = n_x + n_y + n_z$.

The position and rotation of the pipe element in space and time is then obtained by summation,

$$\mathbf{p}_t^0(z,t) = \mathbf{r}(t) + \mathbf{R}_1^0\mathbf{N}(s)\mathbf{q}_e(t),\ \phi(z,t) = \theta(t) + \mathbf{Y}(s)\mathbf{q}_\psi(t) \tag{10}$$

at each sample time and $\phi(z,t)$ is the point at $s = z/L$.

The velocity of the material point on the pipe element can be derived in terms of the generalized coordinates as

$$\dot{\mathbf{p}}_t^0(\mathbf{q}, \dot{\mathbf{q}}) = \left[\mathbf{I}\ \mathbf{H}(\mathbf{q})\ \mathbf{R}_1^0\mathbf{N}\ \mathbf{S}\mathbf{Y}\right]\dot{\mathbf{q}} \tag{11}$$

where $\mathbf{I}$ is the identity matrix, $\mathbf{H}(\mathbf{q}) = \mathbf{B}_\theta(\mathbf{q}) + \mathbf{S}_\theta$, and $\mathbf{q} = \left[\mathbf{r}^\top,\, \theta,\, \mathbf{q}_e^\top,\, \mathbf{q}_\psi^\top\right]^\top$ are the drill-string generalized coordinates. The configuration gives a total set of $n_q = \dim(\mathbf{r}) + n_{\text{modes}} + 1$ generalized coordinates.

SYSTEM ENERGY

The energy of a pipe segment dz is comprised of kinetic energy due to linear and angular velocity, and potential energy in form of strain energy and gravitational potential energy. The kinetic energy T of the material point on the pipe disc dz is given by

$$T = \frac{1}{2}\int_p \dot{\mathbf{p}}_t^{0^\top}\dot{\mathbf{p}}_t^0 \mathrm{d}m \tag{12}$$

We further assume that the density and cross-sectional area of the pipe is uniform over the entire length. Integrating (12) around the pipe circumference for each mass point $\mathbf{p}_t^0$, then integrating along the pipe axis z gives the total kinetic energy. The infinitesimal area is derived according to Fig. 3 as $\mathrm{d}A = \tilde{r}t_w\,\mathrm{d}\alpha$, where α is an arc angle and t_w is the pipe wall thickness. The element volume is then $\mathrm{d}V = \mathrm{d}A\mathrm{d}z$ and the mass element $\mathrm{d}m$ is defined as $\mathrm{d}m = \rho\mathrm{d}V = \rho t_w\tilde{r}\mathrm{d}\alpha\mathrm{d}z$. This allows us to rewrite (12) in terms of the generalized coordinates as

$$T = \frac{1}{2}\dot{\mathbf{q}}^\top\mathbf{M}\dot{\mathbf{q}} \tag{13}$$

where $\mathbf{M} = \mathbf{M}^\top$ is the system mass matrix for the pipe element, i.e.,

$$\mathbf{M} = \tilde{r}\rho t_w\int_z\int_\alpha \begin{bmatrix} \mathbf{I} & \mathbf{H} & \mathbf{R}_1^0\mathbf{N} & \mathbf{S}_\psi\mathbf{Y} \\ \dots & \mathbf{H}^\top\mathbf{H} & \mathbf{H}^\top\mathbf{R}_1^0\mathbf{N} & \mathbf{H}^\top\mathbf{S}_\psi\mathbf{Y} \\ \dots & \dots & \mathbf{N}^\top\mathbf{N} & \mathbf{N}^\top\mathbf{R}_1^{0\top}\mathbf{S}_\psi\mathbf{Y} \\ \dots & \dots & \dots & \mathbf{Y}^\top\mathbf{S}_\psi^\top\mathbf{S}_\psi\mathbf{Y} \end{bmatrix}\mathrm{d}\alpha\mathrm{d}z \tag{14}$$

where $\mathbf{R}^\top\mathbf{R} = \mathbf{I}$ has been used. The dimension of the mass matrix is $n_q \times n_q$, and depends on the number of generalized coordinates. The moment of inertia of the pipe is then the integrated element $J = \mathbf{H}^\top\mathbf{H}$.

The potential energy due to strain from deformation of the element is due to the property of the pipe to resist deformation. The strain energy of the element can be defined for each of the distinctive axes in frame $\{2\}$ according to [17], yielding

$$U_x = \tfrac{1}{2}EI\left(\tfrac{\partial^2 u_{1e}}{\partial z^2}\right)^2,\ U_y = \tfrac{1}{2}EI\left(\tfrac{\partial^2 u_{2e}}{\partial z^2}\right)^2 \tag{15}$$

$$U_z = \tfrac{1}{2}EA\left(\tfrac{\partial u_{3e}}{\partial z}\right)^2,\ U_\psi = \tfrac{1}{2}GI\left(\tfrac{\partial \psi}{\partial z}\right)^2 \tag{16}$$

where the products EI is the flexural rigidity for x, y, EA is the axial rigidity and GI is the torsional rigidity. Using the definition of $\mathbf{p}_e(z,t)$ from (8), we can express the derivatives with respect to z as

$$\frac{\partial\mathbf{p}_e^1}{\partial z} = \frac{1}{L}\mathbf{N}'\mathbf{q}_e,\ \frac{\partial^2\mathbf{p}_e^1}{\partial z^2} = \frac{1}{L^2}\mathbf{N}''\mathbf{q}_e,\ \frac{\partial\psi}{\partial z} = \frac{1}{L}\mathbf{Y}'\mathbf{q}_r \tag{17}$$

where the prime $'$ and $''$ represent first and second derivative with respect to z. The strain energy due to bending, longitudinal stress, and torsion using (17) yields

$$\begin{aligned} U = &\frac{1}{2}\mathbf{q}_x^\top\frac{EI}{L^3}\int_0^1\mathbf{N}_x''^\top\mathbf{N}_x''\mathrm{d}s\,\mathbf{q}_x + \mathbf{q}_y^\top\frac{EI}{L^3}\int_0^1\mathbf{N}_y''^\top N_y''\,\mathrm{d}s\,\mathbf{q}_y \\ &+\mathbf{q}_z^\top\frac{EA}{L}\int_0^1\mathbf{N}_z'^\top\mathbf{N}_z'\mathrm{d}s\,\mathbf{q}_z + \mathbf{q}_r^\top\frac{GI}{L}\int_0^1\mathbf{Y}'^\top\mathbf{Y}'\,\mathrm{d}s\,\mathbf{q}_r \end{aligned} \tag{18}$$

where $\mathbf{N}_j$ are the row vectors from (9). Taken the advantage of equal mode shape functions for lateral deformation, $\mathbf{N}_x'' = \mathbf{N}_y''$, we can write the total strain potential energy as

$$U = \frac{1}{2}\left(\mathbf{q}_x^\top\mathbf{K}_1\mathbf{q}_x + \mathbf{q}_y^\top\mathbf{K}_2\mathbf{q}_y + \mathbf{q}_z^\top\mathbf{K}_3\mathbf{q}_z + \mathbf{q}_r^\top\mathbf{K}_\psi\mathbf{q}_r\right). \tag{19}$$

The total strain energy in matrix form can be written as

$$U_e = \frac{1}{2}\mathbf{q}^\top\begin{bmatrix}\mathbf{0} & \mathbf{0} & \mathbf{0} & \mathbf{0} \\ \mathbf{0} & 0 & \mathbf{0} & \mathbf{0} \\ \mathbf{0} & \mathbf{0} & \mathbf{K}_e & \mathbf{0} \\ \mathbf{0} & \mathbf{0} & \mathbf{0} & \mathbf{K}_\psi\end{bmatrix}\mathbf{q} = \frac{1}{2}\mathbf{q}^\top\mathbf{K}\mathbf{q} \tag{20}$$

where $\mathbf{K} = \mathbf{K}^\top$, and the stiffness matrix $\mathbf{K}_e = \mathrm{diag}(\mathbf{K}_1, \mathbf{K}_2, \mathbf{K}_3)$. The gravitational potential energy is derived in form of an external force in the next section, and not included in the total potential energy.

EXTERNAL AND APPLIED FORCES AND TORQUES

The external forces acting on the body are the gravitational force and impact force from the borehole wall. Since we consider a pipe deformation which is subject to lateral movement with no rotation around y_2 or x_2, we assume that z_1 and z_2 are oriented vertically downwards. The gravitational force acting on $\mathrm{d}m$ is $\mathbf{F}_g = \begin{bmatrix}0,\ 0,\ g\mathrm{d}m\end{bmatrix}^\top$ and the virtual work of the gravitational force acting on each point on the pipe is given by

$$\delta W_g^e = \mathbf{F}_g^\top\delta\mathbf{p}_t^0 \tag{21}$$

where the virtual displacement is given by

$$\delta\mathbf{p}_t^0 = \sum_{k=1}^{n_q}\frac{\partial\mathbf{p}_t^0}{\partial q_k}\delta q_k = \begin{bmatrix}\mathbf{I},\ \mathbf{H}(\mathbf{q}),\ \mathbf{R}_1^0\mathbf{N},\ \mathbf{S}_\psi\mathbf{Y}\end{bmatrix}\delta\mathbf{q} = \mathbf{L}\delta\mathbf{q} \tag{22}$$

where $\mathbf{L} = \begin{bmatrix}\mathbf{I},\ \mathbf{H}(\mathbf{q}),\ \mathbf{R}_1^0\mathbf{N},\ \mathbf{S}_\psi\mathbf{Y}\end{bmatrix}$. Integrating the virtual work for $\mathrm{d}m$ over the entire length of the string yields

$$\delta W_g^e = \tilde{r}\rho t_w L\int_0^1\int_0^{2\pi}\mathbf{F}_g^\top\begin{bmatrix}\mathbf{I},\ \mathbf{H}(\mathbf{q}),\ \mathbf{R}_1^0\mathbf{N},\ \mathbf{S}_\psi\mathbf{Y}\end{bmatrix}\mathrm{d}\alpha\mathrm{d}s\delta\mathbf{q}. \tag{23}$$

Inspecting this integral, we find that the last row of $\mathbf{H}$ is zero and the product $\mathbf{F}_g^\top \mathbf{R}_1^0 \mathbf{N}$ evaluates to a row vector $[\mathbf{0}, \mathbf{N}_z]$. We can then simplify (23) as

$$\boldsymbol{\tau}^e = 2\pi\tilde{r}\rho L \left[\left[0,\, 0,\, g\right],\, 0,\, [\mathbf{0}, g\mathbf{N}_z],\, \mathbf{0} \right]^\top \tag{24}$$

where $\boldsymbol{\tau}_g^e$ is the vector generalized gravitational forces.

The drill-string is subject to lateral motion and hence is constrained by the borehole wall. For the interactions occurring while drilling we shall assume that the deformation of the borehole wall is negligible, and we only consider the impact response, i.e., the contact forces that occur when the string hits the wall.

The impact with the wall is modeled by a set of springs which set up a reaction force. This is seen in the lower section of Fig. 1. In this paper, the contact dynamics are adopted from the Hertzian contact law in [8]. Referring to Fig. 1, the impact occurs when the lateral displacement of the drill-string is larger than the clearance variable l_c. The discontinuous function for lateral displacement in the x direction is defined as

$$F_{c,j}(z,t) = \begin{cases} -k_c(-m(z,t) - l_c)^{3/2}, & m(z,t) \le -l_c \\ 0, & -l_c \le m(z,t) \le l_c \\ k_c(m(z,t) - l_c)^{3/2}, & m(z,t) \ge l_c \end{cases} \tag{25}$$

where $m(z,t)$ is given by the position of the drill-string at z for a given time. The expression in (25) is also defined in similar manner for the y axis.

The generalized force governing the Hertzian contact law for point i along the z axis in the borehole can then be derived as

$$\boldsymbol{\tau}_{c,i}^e = \int_0^1 \int_0^{2\pi} \mathbf{F}_c{}^\top \mathbf{L} \delta(s - \frac{z_i}{L}) \mathrm{d}\alpha \mathrm{d}s \tag{26}$$

where $\delta(s - \frac{z_i}{L})$ is the Dirac delta function and $\mathbf{F}_c = [F_{cx}, F_{cy}, 0]^\top$ is the vector of contact forces.

Non-conservative forces

Viscous damping is included to simulate the dissipation of energy in the vibrating body. The viscous damping in vertical wells includes the effect of drilling mud between the borehole and string [11]. The damping matrix is defined as $\mathbf{D} = \mathrm{diag}(R_1, R_2, \ldots, R_i)$. Following [18], that each structure dissipates energy when excited, we define the structural damping R_i for each mode as

$$R_q = 2\xi_e \sqrt{k_i m_i},\ R_\psi = 2\xi_\psi \sqrt{c_i J_i} \tag{27}$$

where ξ is the damping ratio, k_i is the equivalent stiffness for axial and lateral modes, c_i is the equivalent torsional stiffness, and J_i is the modal moment of inertia. The vector of damping forces is then $\boldsymbol{\tau}_{\mathrm{nc}}^d = -\mathbf{D}\dot{\mathbf{q}}$, with subscript nc for non-conservative.

Actuating Forces

The actuating forces are the forces at the top of the pipe due to hoisting or lowering, and the applied torque on the pipe. The vector $\mathbf{F}^0 = [F_x, F_y, F_z]^\top$ is the vector of actuating forces expressed in the inertial frame. The two forces perpendicular to the element on the x and y axis are restoring forces, which hold the pipe in place. The definition of the forces acting on the pipe element is illustrated in Fig. 4.

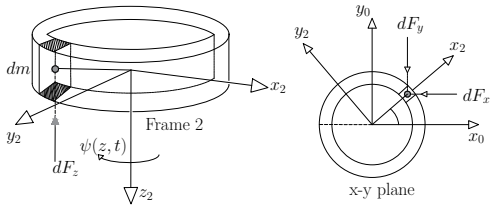

FIGURE 4. DISTRIBUTED FORCES

The forcing function directing $\mathbf{F}^0$ to the point z_p on the pipe is the Dirac function $\delta(s - \frac{z_i}{L})$. The virtual work of the actuating forces for $\mathbf{F}^0$ is derived in similar manner as (26), yielding

$$\boldsymbol{\tau}_f^{a\top} = \int_0^1 \int_0^{2\pi} \mathbf{F}^{0\top} \mathbf{L} \delta(s - \frac{z_p}{L}) \mathrm{d}\alpha \mathrm{d}s \tag{28}$$

Since the Dirac function is used to only evaluate the integral when $s = \frac{z_p}{L}$, we can rewrite (28) as

$$\boldsymbol{\tau}_f^{a\top} = \mathbf{F}^{0\top} \boldsymbol{\Gamma}(z_p, \mathbf{q}) \tag{29}$$

where $\boldsymbol{\Gamma}(z_p, \mathbf{q}) = 2\pi \mathbf{L}(\frac{z_p}{L})$

The applied torque on the pipe is assumed to independently interact with θ and ψ. We then define the virtual work of the torque and the generalized torque as

$$\delta W_t^a = T^0 \mathbf{W} \delta \mathbf{q},\ \boldsymbol{\tau}_t^{a\top} = T^0 \boldsymbol{\Lambda}(z_p) \tag{30}$$

where T^0 is a scalar, $\mathbf{W} = \left[\mathbf{0},\, 1,\, \mathbf{0},\, \mathbf{Y}\right]$, $\boldsymbol{\tau}_t^{a\top}$ is the generalized torque and $\boldsymbol{\Lambda}(z_p) = \int_0^1 \mathbf{W} \delta(s - \frac{z_p}{L}) \mathrm{d}s$.

EQUATIONS OF MOTION

The Lagrangian of the system is defined as $L = T - U$. Inserting for the kinetic and strain potential energy into the Lagrangian yields

$$L = \frac{1}{2}\dot{\mathbf{q}}^\top \mathbf{M}(\mathbf{q})\dot{\mathbf{q}} - \frac{1}{2}\mathbf{q}^\top \mathbf{K}\mathbf{q}. \tag{31}$$

The equations of motion for the system is then derived according to the expression

$$\frac{\mathrm{d}}{\mathrm{d}t}\frac{\partial L}{\partial \dot{q}_k} - \frac{\partial L}{\partial q_k} = \tau_k \tag{32}$$

where τ_k is a generalized force. This gives a set of k ODEs for the system. Performing the partial differentiation and taking the time derivative of $\frac{\partial L}{\partial \dot{q}_k}$ yields the expression

$$\mathbf{M}(\mathbf{q})\ddot{\mathbf{q}} + \mathbf{C}(\mathbf{q},\dot{\mathbf{q}})\dot{\mathbf{q}} + \mathbf{K}\mathbf{q} = \boldsymbol{\tau} \tag{33}$$

where $\mathbf{M}\ddot{\mathbf{q}}$ is due to inertial acceleration of the element, $\mathbf{C}(\mathbf{q},\dot{\mathbf{q}})$ is the Coriolis-centripetal forces matrix, and $\boldsymbol{\tau}$ is the generalized forces and torques, $\mathbf{M}$ and $\mathbf{K}$ are given in (14) and (20). The elements of the $\mathbf{C}$ matrix is according to [19], given as

$$c_{k,j} = \sum_{i=1}^{n} \frac{1}{2}\left(\frac{\partial m_{k,j}}{\partial q_i} + \frac{\partial m_{k,i}}{\partial q_j} - \frac{\partial m_{i,j}}{\partial q_k}\right)\dot{q}_i \tag{34}$$

where the length of k, i and j is equal to the number of generalized coordinates. Finally, $\boldsymbol{\tau}$ is defined as

$$\boldsymbol{\tau} = \boldsymbol{\tau}_g^e + \boldsymbol{\tau}_f^a(\mathbf{F}^0) + \boldsymbol{\tau}_t^a(T^0) + \boldsymbol{\tau}_c^e(\mathbf{F}_c) + \boldsymbol{\tau}_{\mathrm{nc}}^d(\dot{\mathbf{q}}). \tag{35}$$

BOND GRAPH MODEL

To formulate the equations of motion in a component-based framework, we utilize the structure of BG elements. A bond graph model is derived from (33), according to the generalized momentum p and displacement q in Hamiltonian form [20]. This gives a field representation of the system. The time derivative of the momentum is given as

$$\dot{p}_k = \frac{d}{dt}\frac{\partial T}{\partial \dot{q}_k} = \frac{\partial T}{\partial q_k} - \frac{\partial U}{\partial q_k} + \tau_k, \;\; \dot{p}_k = e_k^{'} + \tau_k \tag{36}$$

where $e_k^{'}$ is the corresponding effort for inertia forces such as Coriolis forces and the forces and torques due to the stiffness of the system. The generalized momentum and corresponding velocities are then derived as

$$\mathbf{p} = \mathbf{M}\dot{\mathbf{q}}, \;\; \dot{\mathbf{q}} = \mathbf{M}^{-1}\mathbf{p} \tag{37}$$

The gravitational force is represented as an effort source S_e and the damping from $\boldsymbol{\tau}_{\mathrm{nc}}^d$ is modeled as an attached R element. The external forces acting on the model is distributed with a modulated transformer, denoted *MTF*, with modulus $\boldsymbol{\Gamma}(\mathbf{q})$ and $\boldsymbol{\Lambda}$. This constitutive relation holds if the transformer is power conservative, yielding $\mathbf{F}\dot{\mathbf{x}} = \boldsymbol{\tau}_{\mathrm{out}}\dot{\mathbf{q}}_{\mathrm{out}}$ [18].

The final causal BG model for the drill-string component is shown in Fig. 5. The graph has complete integral causality, constraining the subsystems to supply effort as input. This is the advantage of utilizing the BG methodology, where the complex model is formed and now any relevant subsystem can be attached to the model. Note that the bond $[\mathbf{e}_1, \mathbf{f}_1]^\top$ is split into $[\mathbf{e}_5, \mathbf{f}_5]^\top$ and $[\mathbf{e}_2, \mathbf{f}_2]^\top$.

SIMULATIONS

In this section, we investigate the model performance through three simulation case studies; analyzing the input effect on the individual mode shapes, performing tracking of defined revolutions-per-minute (RPM) set-points and the effect of reducing the number of modes. Initially, we define our system with four modes in $u_{j,e}$ and with two torsional modes in ψ. This gives a set of 18 generalized coordinates for the system. The drill-string parameters used in this section are presented in Table 1.

We start by simplifying the expression for the twist $\mathbf{R}_\psi$, enabling easier pre-calculation of the system matrices. The range of the twist angle determines the number of terms for the Taylor series expansion of cosine and sine in the rotation matrix. A consequence of including more terms is increased computational

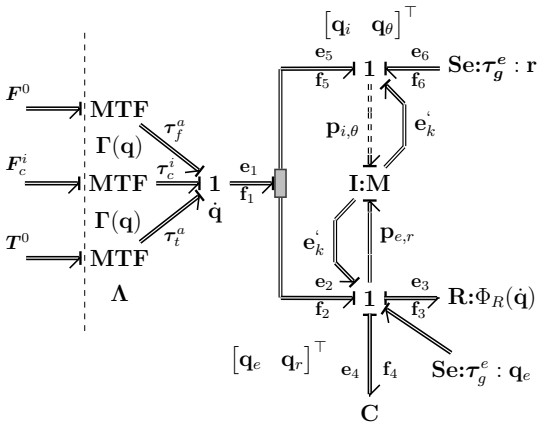

FIGURE 5. BG MODEL OF FLEXIBLE DRILL-STRING

TABLE 1. PIPE STRUCTURAL PARAMETERS

L[m]	ρ [$\frac{\text{kg}}{\text{m}^3}$]	OD [m]	ID [m]	t_w [m]	$\tilde{r}$ [m]	E [GPa]	G [GPa]	g [$\frac{\text{m}}{\text{s}^2}$]
1200	7850	0.125	0.107	0.018	0.058	200	79.3	9.81

time before and in simulation. In this paper we utilize 4th-order expansion of the cosine and 3rd-order expansion of sine, which limits the torsional twist of in the range of $-\frac{3\pi}{2} < \psi(z,t) < \frac{3\pi}{2}$.

The top drive torque system is modeled with a drive inertia and a PID controller, simulating the torque motor. This system is defined as

$$I_{\text{td}}\dot{\omega} = T_m - \frac{T_0}{k_g} - R_d\omega \tag{38}$$

where I_{td} is the drive inertia, T_m is the torque produced by the PID controller, T_0 is the pipe torque, k_g is the gear ratio from the drive to the pipe, and R_d is the damping factor in the drive. The top drive dynamics are implemented as a bond graph model, connected as shown in Fig. 5. Hence, ω is the inertial top drive angular velocity, being transformed to the pipe with $\mathbf{\Lambda}$. We use a stiff controller with $K = 10\zeta_d$, $K_i = 5I_{\text{td}}$, a form commonly applied in early rotary drilling systems [21], where the gain is set by the drill-string pipe characteristic impedance $\zeta_d = I\sqrt{G\rho}$. Furthermore, I is the pipe polar moment of area. The derivative time is set to $t_d = 0.1$ s.

The force input in the lateral and vertical plane is set in the inertial reference frame and transformed to the generalized coordinates by $\tau = \left[F_x^i, F_y^i, F_z^i\right]\mathbf{\Gamma}(\mathbf{q})$. Viscous damping is included in the system at the end of the string, i.e., $z = L$, given as $T_f = \dot{\psi}(z,t)R_f$, where $\dot{\psi}(z,t) = \partial\psi(z,t)/\partial t$ and R_f is chosen to reflect the hydrodynamic damping and geometry of the borehole due to mud and friction.

The system is modelled with proportional damping from (27). Furthermore, the damping coefficients ξ_i are chosen experimentally to simulate damped oscillations of the vibratory modes. Initially $\xi_{x,y} = 0.01$, $\xi_z = 0.1$, $\xi_\psi = \{0.1, 0.2\}$.

The contact forces from $\boldsymbol{\tau}^e_{c,i}$ define the boundary to the wellbore, starting at $z = 300$ m being distributed by 8 contact points, and $l_c = 0.1$ m, $k_c = 2500 \cdot 10^3$ N/m are taken from [7, 22].

Case 1: To evaluate the modal contribution, we perform a spin up test to $\omega_{\text{sp}} = 5$ rad/s, simulating the model for 20 seconds. The number of modes required depends on how accurately we want to capture the frequencies being excited by the system. Since the longitudinal deformation is uncoupled from the lateral and torsional deformation we analyze the results of actuating the string in the vertical direction. The results in terms of root-mean-square (RMS) values describing the individual effect on each mode is listed in Table 2.

From the numbers in Table 2, we can see that the first modes

TABLE 2. MODE RMS VALUES

Mode num.	RMS($\mathbf{q}_{e,x}$)	RMS($\mathbf{q}_{e,y}$)	RMS($\mathbf{q}_{e,z}$)	RMS($\mathbf{q}_{e,r}$)
1	1.094	0.8128	0.9566	1.124
2	0.03408	0.1516	0.03874	0.1244
3	0.08707	0.008734	0.009336	N/A
4	0.02765	0.02692	0.003668	N/A

are excited the most by the input from the top drive and the dynamics of the actuator for the vertical direction at $z = 0$. The modes are based unforced response at the end boundary. However, a drill-string is normally in tension and the drill-collar section is compressed when placed on the rock-bottom. In the following cases, we only consider the results in terms of off-bottom rotation, with no interaction with vertical forces at the end boundary.

The twist angle $\psi(z,t)$ and the twist angular velocity $\dot{\psi}(z,t)$ are seen in Fig. 6. The angle of twist reaches steady-state, and the angular velocity along the drill-string becomes uniform.

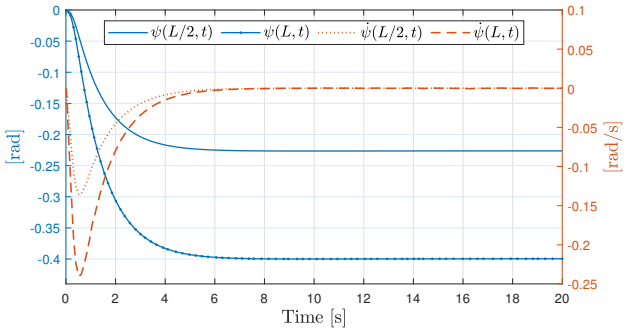

FIGURE 6. TWIST ANGLE AND ANGULAR VELOCITY.

Case 2: In this case we set four individual set-points for ω at 4, 8, 16 and 20 rad/s (38 to 191 RPM approximately). The result is seen in Fig. 7.

The plot shows a first-order response and a small lag in ω_L due to the torsional rigidity of the pipe. The qualitative response is similar to the n-degree 2nd-order lumped models, where the time period of a shear wave is $t_s = \frac{2\pi\sqrt{\rho}}{\sqrt{G}}$ being approximately 0.002 s. Seen in the top-most plot in Fig. 7 is small oscillations for the angular velocity at the bottom of the well. This linked to the lateral motion, which is seen at the boundary $z = L$ in Fig. 8 for $\omega = 4$ rad/s and 20 rad/s.

The lateral displacement at the end of the pipe is oscillating with larger amplitude and frequency for higher RPMs. At this stage we have not considered the effect of added mass and the effect of fluid in the annulus. It is reasonable to think that the effects would provide additional damping.

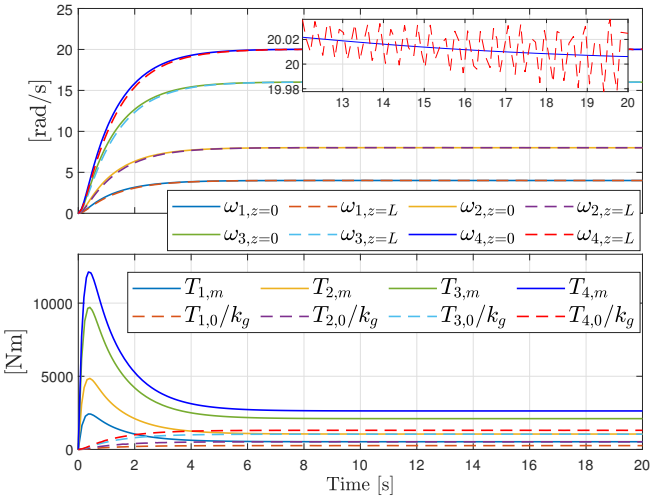

FIGURE 7. ANGULAR VELOCITY AT $z = 0$ AND $z = L$ AND CORRESPONDING DRIVE TORQUE.

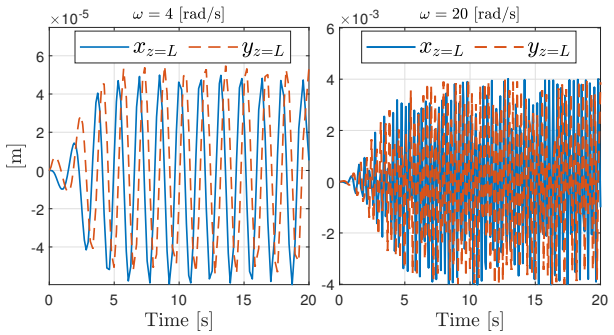

FIGURE 8. LATERAL DISPLACEMENT FOR $\omega = 4$ AND 20 RAD/S.

Case 3: In this case, three different models were developed. Model 1 is equal to the one from the previous cases. Model 2 is developed with 14 degrees of freedom (DOF), three coordinates each in $u_{j,e}$ and one in ψ. Model 3 consist of 12 DOFs, with two coordinates each in $u_{j,e}$ and ψ. The results of simulating for five seconds is seen in Fig. 9. The proportional gain of the drive is increased by a factor of 10, and the inertia is reduced from 90 to 80 kg $\cdot$ m^2. A model parameter change is made for the resisting torque from viscous damping at $z = L$, where the coefficient is increased from 65 to 80 $\frac{\text{N}\cdot\text{m}\cdot\text{s}}{\text{rad}}$.

The upper-most and lower-most plots indicate that the trajectories correspond to the findings in Table 2, where the three first modes play a significant role in the magnitude of lateral deformation. Less effect is seen on the torsional deformation, corresponding to one or two modes. The deviation seen in the lowermost figure is approximately 0.0019 m.

In terms of simulation performance, we can evaluate the ratio of simulation time to actual time defined as $t_{\text{rt}} = t_{\text{a}}/t_{\text{sim}}$, where t_{a} is the actual time. The ratio resulted in $t_{\text{rt}} = 10.56$ (Model 1), $t_{\text{rt}} = 1.47$ (Model 2), and $t_{\text{rt}} = 7.82$ (Model 3). Model 1 and 3 have two coordinates in ψ, while Model 2 has one; the size reduction in model matrices explains the difference in speed. Model 2 is then assumed to be better suited for real-time applications.

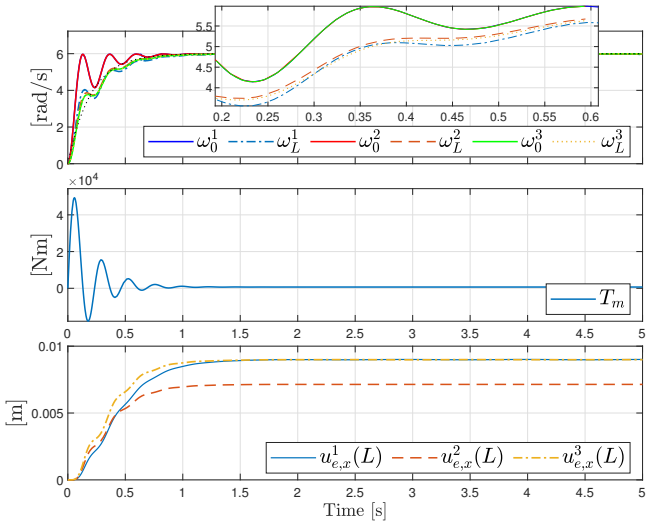

FIGURE 9. SIMULATION OF THREE MODELS $n_q = 18$, 14 AND 12. THE ANGULAR VELOCITIES ARE ω_0, ω_L AT $z = 0$ AND $z = L$ RESPECTIVELY, AND $u_{1,e}$ IS THE X AXIS DEFORMATION.

CONCLUSIONS

In this paper we have derived a drill-string model with coupled torsion and lateral motion in terms of the floating frame of reference formulation, and additionally shown a component-based structure of a drill-string model. The model was incorporated in a bond graph structure, where full integral causality is ensured with the IC framework.

To limit the computational time and avoid numeric integration to obtain the mass matrix in terms of the non-dimensional parameter s, the rotation matrix R_ψ was approximated by a 3rd and 4th order Taylor series expansion for sine and cosine, respectively, which showed to have advantages for the reduced degree of freedom Model 2 in terms of simulation time.

The model performance was tested in three simulation cases, analyzing the total modal contribution, showing that the first mode of the generalized coordinates was influenced the most by the top drive dynamics. Limiting the number of modes through geometry conditions and required accuracy is shown to improve simulation speed towards real-time applications.

The model is component-based-oriented, including the dynamics of torsional, lateral, and longitudinal motion being able

to be used in large scale simulation case studies. Further analysis of the dynamics of the model should incorporate the stick-slip effect. Therefore, new implementation with the exact rotation matrix $\mathbf{R}_\psi$ should be done. However, this will likely lead to increased simulation time.

Future work

We have shown that it is possible to model pipe twist in relation to the lateral motion, achieving a model capturing the coupled phenomena without relying on bit-rock interaction models. However, validity of the proposed model is key to further use in industry. The validity must be tested towards real-world measurements and cross checked with existing models to best estimate the nonlinear drill-string dynamics. The simulation showed the coupling effect of torsional and lateral deformation. A control design approach should be derived in terms of stabilizing the dynamics of the drill-string. Hence, testing existing control laws on this model can give valuable insight of controller performance. However, this was not the objective of this paper, and remains future work.

ACKNOWLEDGMENT

The research presented in this paper has received funding from the Norwegian Research Council, SFI Offshore Mechatronics, project number 237896.

REFERENCES

[1] Kapitaniak, M., Vaziri Hamaneh, V., Chávez, J. P., Nandakumar, K., and Wiercigroch, M., 2015. "Unveiling complexity of drill-string vibrations: Experiments and modelling". *International Journal of Mechanical Sciences,* ***101-102***, pp. 324–337.

[2] Ritto, T. G., Soize, C., and Sampaio, R., 2009. "Non-linear dynamics of a drill-string with uncertain model of the bit-rock interaction". *International Journal of Non-Linear Mechanics,* ***44***(8), pp. 865–876.

[3] Kyllingstad, Å., and Halsey, G. W., 1988. "A Study of Slip/Stick Motion of the Bit". *SPE Drilling Engineering,* ***3***(4), pp. 369–373.

[4] Tucker, R., and Wang, C., 2003. "Torsional Vibration Control and Cosserat Dynamics of a Drill-Rig Assembly". *Meccanica,* ***38***(1), pp. 143–159.

[5] Jansen, D. J., 1993. "Nonlinear Dynamics of Oilwell Drillstrings". PhD thesis, Delft University.

[6] Richard, T., Germay, C., and Detournay, E., 2007. "A simplified model to explore the root cause of stick-slip vibrations in drilling systems with drag bits". *Journal of Sound and Vibration,* ***305***(3), pp. 432–456.

[7] Christoforou, A. P., and Yigit, A. S., 2003. "Fully coupled vibrations of actively controlled drillstrings". *Journal of Sound and Vibration,* ***267***(5), pp. 1029–1045.

[8] Spanos, P. D., Chevallier, A. M., and Politis, N. P., 2002. "Nonlinear Stochastic Drill-String Vibrations". *Journal of Vibration and Acoustics,* ***124***(4), p. 512.

[9] Bakhtiari-Nejad, F., and Hosseinzadeh, A., 2017. "Nonlinear dynamic stability analysis of the coupled axial-torsional motion of the rotary drilling considering the effect of axial rigid-body dynamics". *International Journal of Non-Linear Mechanics,* ***88***(June 2016), pp. 85–96.

[10] Detournay, E., and Defourny, P., 1992. "A phenomenological model for the drilling action of drag bits". *International Journal of Rock Mechanics and Mining Sciences and Geomechanics,* ***29***(1), pp. 13–23.

[11] Hovda, S., 2018. "Semi-analytical model of the axial movements of an oil-well drillstring in deviated wellbores". *Journal of Sound and Vibration,* ***433***, pp. 287–298.

[12] Borutzky, W., 2009. "Bond graph modelling and simulation of multidisciplinary systems - An introduction". *Simulation Modelling Practice and Theory,* ***17***(1), pp. 3–21.

[13] Pedersen, E., and Polic, D., 2014. "Bond graph modeling of rotordynamic systems with a flexible shaft including shear correction". *In proc. from International Conference on Bond Graph Modeling, ICBGM 2014,* ***46***, pp. 205–212.

[14] Sarker, M., Rideout, D. G., and Butt, S. D., 2017. "Dynamic model for 3D motions of a horizontal oilwell BHA with wellbore stick-slip whirl interaction". *Journal of Petroleum Science and Engineering,* ***157***, pp. 482–506.

[15] Shabana, A. A., 2013. *Dynamics of multibody systems*. Cambridge university press.

[16] Rao, S. S., 2007. *Vibration of Continuous Systems*. John Wiley & Sons.

[17] Pacoste, C., and Eriksson, A., 1997. "Beam elements in instability problems". *Computer Methods in Applied Mechanics and Engineering,* ***144***(1-2), pp. 163–197.

[18] Karnopp, D. C., Margolis, D. L., and Rosenberg, R. C., 2012. *System dynamics: modeling, simulation, and control of mechatronic systems*. John Wiley & Sons.

[19] Egeland, O., and Gravdahl, J. T., 2002. *Modeling and Simulation for Automatic Control*, Vol. 76. Marine Cybernetics Trondheim, Norway.

[20] Karnopp, D., 1982. "Dynamic forces in multiport mechanics: Direct and Lagrangian formulations". *Journal of the Franklin Institute,* ***314***(5), pp. 265–270.

[21] Kyllingstad, Å., and Nessjøen, P. J., 2009. "A New Stick-Slip Prevention System". *SPE/IADC Drilling Conference and Exhibition*(March), pp. 17–19.

[22] Spanos, P. D., Sengupta, A. K., Cunningham, R. A., and Paslay, P. R., 1995. "Modeling of Roller Cone Bit Lift-Off Dynamics in Rotary Drilling". *Journal of Energy Resources Technology,* ***117***(3), p. 197.